JPhys Materials

OPEN ACCESS

RECEIVED
24 April 2019

REVISED
5 June 2019

ACCEPTED FOR PUBLICATION
13 June 2019

PUBLISHED
6 August 2019

PAPER

Potassium titanyl phosphate (KTP) quasiparticle energies and optical response

S Neufeld, A Bocchini, U Gerstmann, Arno Schindlmayr and W G Schmidt

Department Physik, Universität Paderborn, 33095 Paderborn, Germany

E-mail: sergejn@mail.upb.de

Keywords: DFT, GW, BSE, potassium titanyl phosphate, $KTiOPO_4$, KTP

Abstract

The $KTiOPO_4$ (KTP) band structure and dielectric function are calculated on various levels of theory starting from density-functional calculations. Within the independent-particle approximation an electronic transport gap of 2.97 eV is obtained that widens to about 5.23 eV when quasiparticle effects are included using the *GW* approximation. The optical response is shown to be strongly anisotropic due to (i) the slight asymmetry of the TiO_6 octahedra in the (001) plane and (ii) their anisotropic distribution along the [001] and [100] directions. In addition, excitonic effects are very important: The solution of the Bethe–Salpeter equation indicates exciton binding energies of the order of 1.5 eV. Calculations that include both quasiparticle and excitonic effects are in good agreement with the measured reflectivity.

Introduction

Potassium titanyl phosphate ($KTiOPO_4$, KTP)—a member of the ferroelectric $MAOXO_4$ crystal family—promises numerous technological applications due to its interesting optical properties [1–6]. Its large optical transparency range in conjunction with large electro-optical coefficients and nonlinear susceptibilities [7] are, e.g. exploited for frequency conversion devices [8, 9]. However, the so-called gray tracking, i.e. photochromic damage, limits the usage of KTP. The detailed exploration of the interplay between the material's structural and electronic properties is an essential requirement for its further optimization and possibly the prevention or reduction of photodarkening.

The ferroelectric oxide crystallizes in the orthorhombic space group $Pna2_1$. The unit cell, see figure 1, contains 8 formula units of $KTiOPO_4$, amounting to 64 atoms in total. The O atoms are further subdivided into groups which either bond with Ti and P (O_{TP}) or with two Ti atoms (O_{TT}). The crystal structure is composed of TiO_6 octahedra and PO_4 tetrahedra forming a network of alternating polyhedra chains linked by mutual O corner atoms along the [010] and [100] direction. The titanium atoms within the octahedra exhibit a displacement from the center, which causes alternating long Ti—O and short Ti=O bonds to form [10], as indicated in figure 1. This bond distortion is the main origin of the crystal's internal polarization of 20.1 μC cm^{-2} [11, 12] and its ferroelectricity. Potassium ions are incorporated within the channels in between the polyhedron network, forming weak K—O bonds, and give rise to high ionic conductivity along the channels.

The KTP electronic properties are insufficiently understood. The reported values of the fundamental band gap as concluded from optical measurements range from 3.2 to 3.8 eV [13–17]. Even larger is the range of the computationally predicted band gaps. Density-functional theory (DFT) calculations predict values—depending on the choice of the exchange-correlation functional—of 3.0 [18], 3.1 [13, 19], 3.3 and 4.0 eV [20], whereas early empirical tight-binding calculations obtained a value of 4.9 eV [21]. Both the measured and the calculated values must be taken with caution: on the one hand, the measured values are concluded from optical experiments and are, therefore, affected substantially by electron-hole attraction effects in contrast to the transport band gap, i.e. the difference between the ionization energy and the electron affinity [22–27]. On the other hand, all previous band-structure calculations are based on a single-particle picture and neglect quasiparticle effects that typically

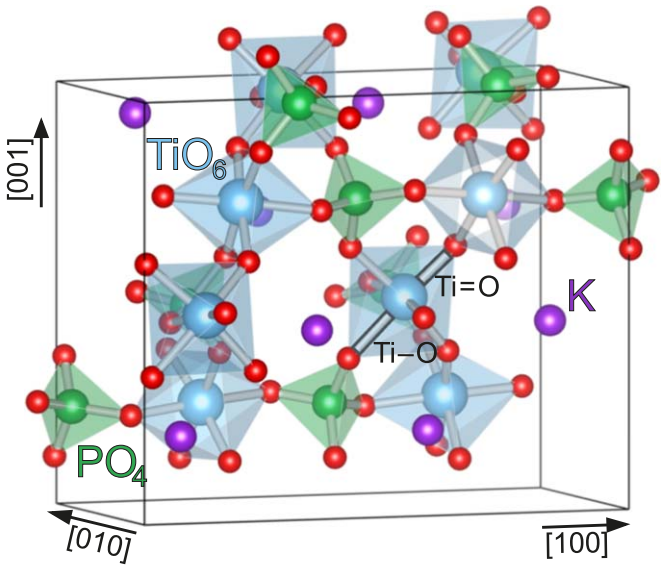

Figure 1. Orthorhombic unit cell of KTP. O atoms coordinating Ti and P ions are linked by polyhedral edges in blue and green, respectively.

widen the band gap between occupied and empty states by a large fraction of its value [28, 29]. The seemingly good agreement between some of the measured and calculated band gaps cited above may thus result from a fortuitous error cancellation between the possibly large exciton binding energy and the electronic self-energy.

The influence of excitonic and local-field effects on the KTP optical absorption is unknown. The existing calculations rely either completely on the independent-particle approximation [20] or use a scissors-operator approach to align the calculated and measured absorption peaks [13].

A better understanding of the KTP excited-state properties is the aim of the present study. To this end, we proceed in three steps: (i) we use DFT to determine the structurally relaxed ground state. (ii) The electronic quasiparticle spectrum is obtained within the *GW* approximation [30] for the exchange-correlation self-energy. (iii) Finally, the Bethe–Salpeter equation (BSE) is solved for coupled electron-hole excitations [31], thereby accounting for the screened electron-hole attraction and the unscreened electron-hole exchange.

Computational method

The ground-state calculations are performed using the Vienna *ab initio* Simulation Package (VASP) [32], an implementation of DFT. The electron exchange-correlation effects are described within the generalized gradient approximation (GGA), using the PBEsol functional [33]. In addition to all open shells, our calculations treat the K 3*p*, Ti 4*s*, P 3*s*, and O 2*s* orbitals as valence states, and we use the projector-augmented-wave technique [34] to describe the electron–ion interaction. The electron wave functions are expanded into plane waves up to an energy cutoff of 500 eV. A Γ-centered $2 \times 4 \times 2$ **k**-point mesh is used to sample the Brillouin zone throughout all calculations, ensuring numerical convergence of the transport gap within less than 10 meV.

In the second step, we include electronic self-energy effects, i.e. we replace the GGA exchange and correlation potential by the nonlocal and energy-dependent self-energy operator $\Sigma(\mathbf{r}, \mathbf{r}'; \omega)$. We calculate Σ in the *GW* approximation [30] from the convolution of the single-particle propagator *G* and the dynamically screened Coulomb interaction *W*, using the implementation of Shishkin and Kresse [35]. The response function is set up using an energy cutoff of 300 eV and a total of 1800 states. Again, this ensures numerical convergence of the quasiparticle energies better than 10 meV. The high computational cost related to the large unit cell and the large number of electronic states mandates a perturbative evaluation of the quasiparticle equation where self-consistency effects are neglected.

The electron-hole interaction is taken into account in the third step, where we solve the BSE [31] that accounts for the interaction of electrons in conduction states and holes in valence states, i.e. excitonic effects, as well as for the electron-hole exchange, i.e. the influence of local fields. For the actual calculation of the polarizability, we use the time-evolution implementation described in [36]. In total, 64 valence and 120 conduction bands are used to set up the two-particle Hamiltonian.

Table 1. Reduced coordinates of non-symmetry-equivalent atoms as obtained within DFT-PBEsol for KTP. In brackets the deviation from single-crystal x-ray diffraction (XRD) data [40] is given. *x*, *y*, and *z* correspond to the [100], [010], and [001] directions, respectively (see figure 1).

	x	*y*	*z*
K(1)	0.375 [−0.003]	0.779 [−0.002]	0.690 [+0.002]
K(2)	0.108 [+0.003]	0.699 [±0]	0.936 [+0.003]
Ti(1)	0.373 [±0]	0.500 [±0]	0.991 [−0.009]
Ti(2)	0.245 [−0.002]	0.260 [−0.01]	0.742 [−0.006]
P(1)	0.498 [±0]	0.339 [+0.003]	0.738 [−0.002]
P(2)	0.180 [−0.001]	0.504 [+0.002]	0.487 [±0]
$O_{TP}(1)$	0.486 [±0]	0.489 [+0.002]	0.849 [−0.001]
$O_{TP}(2)$	0.510 [±0]	0.467 [+0.001]	0.615 [−0.002]
$O_{TP}(3)$	0.401 [+0.001]	0.199 [±0]	0.720 [−0.001]
$O_{TP}(4)$	0.594 [+0.001]	0.196 [+0.003]	0.760 [+0.001]
$O_{TP}(5)$	0.111 [−0.002]	0.314 [+0.003]	0.459 [±0]
$O_{TP}(6)$	0.112 [+0.001]	0.696 [+0.004]	0.513 [+0.001]
$O_{TP}(7)$	0.253 [±0]	0.538 [+0.002]	0.372 [±0]
$O_{TP}(8)$	0.252 [−0.001]	0.465 [+0.003]	0.602 [+0.001]
$O_{TT}(1)$	0.223 [−0.002]	0.966 [+0.001]	0.358 [+0.002]
$O_{TT}(2)$	0.224 [+0.001]	0.051 [+0.01]	0.612 [+0.002]

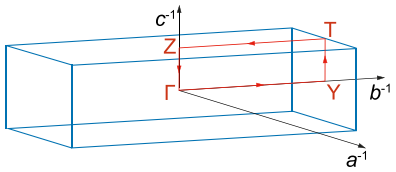

Figure 2. First Brillouin zone of KTP. High-symmetry points as well as the **k**-point path used for the band-structure calculations are indicated.

Results

The KTP lattice constants determined within DFT-PBEsol amount to $a = 12.860$ Å, $b = 6.432$ Å, and $c = 10.599$ Å and deviate by less than 0.4% from the respective experimental data [13, 37–39]. The longest Ti−O and shortest Ti=O bond lengths are calculated to be 2.12Å and 1.78 Å, respectively. Table 1 contains the reduced coordinates of all non-symmetry-equivalent atoms and their deviation from the experimental values [40]. Obviously, DFT-PBEsol provides structural data in remarkably close agreement with the experiment.

The relaxed ground-state structure determined above is used to calculate the electronic band structure along the high-symmetry lines shown in figure 2. For DFT, the corresponding values are shown in figure 3 (lhs). The valence-band maximum (VBM) is located at the T point, slightly (28 meV) above the highest occupied state at Γ. It is separated from the conduction-band minimum (CBM) at Γ by an energy gap of 2.97 eV, in close agreement with earlier DFT–GGA calculations by Lowther *et al* [18]. The VBM and CBM orbital characters are shown in figure 4. They are formed by O 2*p* and Ti 3*d* states, respectively, as is also obvious from the orbital-decomposed density of states in figure 3. A slight increase of the band gap to 3.1 eV is observed upon treating the Ti 3*p* orbitals as valence states (along with an increase of the energy cutoff to 800 eV). However, this is still clearly below the range of experimental values for the band gap concluded from experiments that range from from 3.2 to 3.8 eV [13].

The combined effect of spin–orbit coupling (SOC) and the Coulomb-potential asymmetry related to the ferroelectricity may cause a momentum-dependent splitting of the spin bands which reduces the band gap and causes a Rashba-like spin texture of the electronic structure [41]. Therefore, we also explore the influence of SOC on the band gap, using the VASP implementation [42]. A SOC induced splitting of the valence and conduction bands is found solely for states close to the T point, amounting to 7 meV and 8 meV, respectively. Additionally, the VBM is found to remain at the T point, while the CBM remains at Γ. Thus, the influence of SOC on the band gap is negligible in the present case.

The underestimation of the fundamental gap is a major limitation of DFT [29]. In order to correct the DFT band-gap underestimation, *GW* quasiparticle calculations are performed, see figure 3 (rhs). An essentially

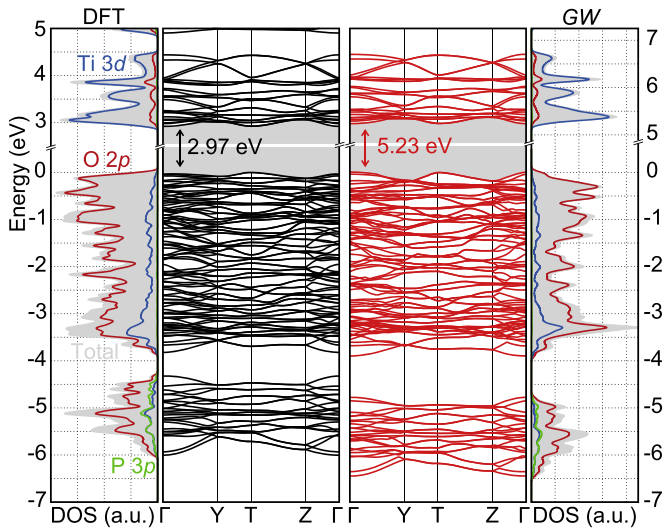

Figure 3. KTP band structures and orbital-decomposed densities of states as calculated within DFT-PBEsol (lhs) and *GW* (rhs). Note the different energy scales.

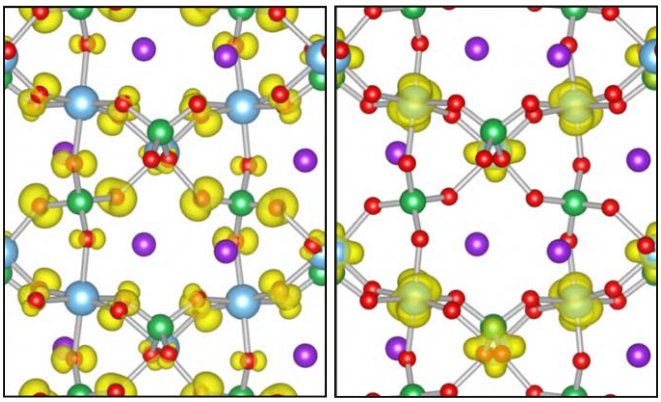

Figure 4. Calculated orbital character of VBM (lhs) and CBM (rhs) states. Color coding as in figure 1: titanium, phosphorus, oxygen, and potassium atoms are indicated in blue, green, red, and purple, respectively.

dispersion-less shift of the valence and conduction states to lower and higher energies, respectively, is observed. In the band-gap region, the respective shifts amount to −0.6 and 1.7 eV. The energy scale in figure 3 is shifted in such a way that the energies of all states in the *GW* band structure refer to the VBM. As a result of the self-energy correction, the electronic band gap widens to 5.23 eV. Additionally, the VBM switches to Γ and is now 8 meV above the highest occupied state at T. Given that self-consistently determined quasiparticle gaps are frequently larger than perturbative non-self-consistent corrections [41, 43] and that the inclusion of Ti 3*p* can be expected to further increase the band gap, we expect the transport gap of 5.23 eV calculated here to represent a lower bound to the actual value.

Based on the electronic structure obtained within DFT-PBEsol and the *GW* approximation, we calculate the frequency-dependent dielectric function in the independent-particle and the independent-quasiparticle approximation (IPA/IQA). The imaginary parts of the three diagonal components of $\varepsilon(\omega)$ are shown in figure 5.

Clearly, the lineshape of the onset of the optical absorption is polarization dependent: in the low-energy range below 4 eV, two distinct peaks can be identified in the imaginary parts of ε_{xx} and ε_{zz} (labeled p_1 and p_2 in figure 5), while a weak shoulder and a pronounced peak characterize ε_{yy}. Additionally, a low intensity peak around 6 eV (labeled p_3) can be identified within all three polarizations. The electronic transitions mainly responsible for the peaks p_1, p_2 and p_3 in the absorption spectrum, i.e. transitions within the respective energy ranges that show strong oscillator strengths, are indicated in figure 6. The absorption onset leading to p_1—most obvious for $\varepsilon_{zz}(\omega)$—is due to transitions from states close to the VBM into electronic bands at or slightly above the CBM. Transitions from states within about 1 eV below the VBM to the CBM, and states about 2 eV above the CBM give rise to p_2 and p_3, respectively. The three most dominant peaks p_1, p_2, and p_3 can thus be traced to

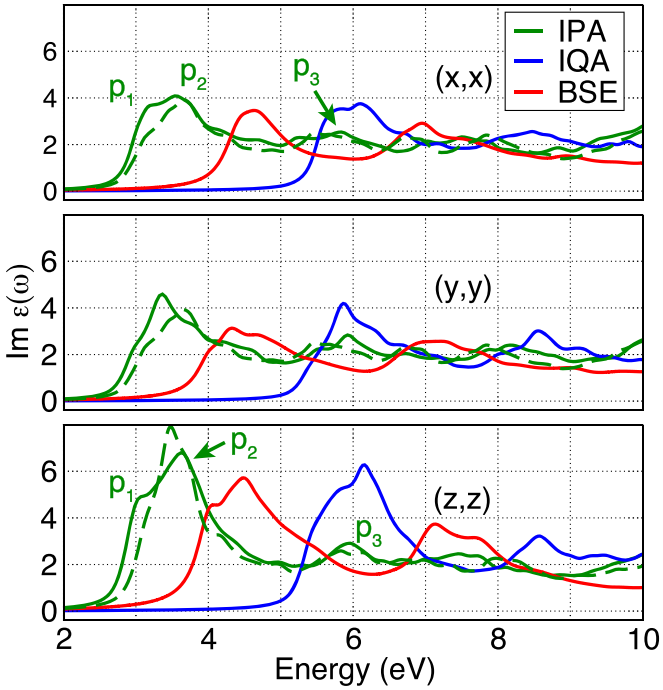

Figure 5. Imaginary part of the diagonal components *xx*, *yy* and *zz* of the KTP dielectric function calculated on the IPA, IQA and BSE level of theory. Dashed curves refer to IPA spectra for the artificial structure shown in figure 7. Some dominant peaks are labeled.

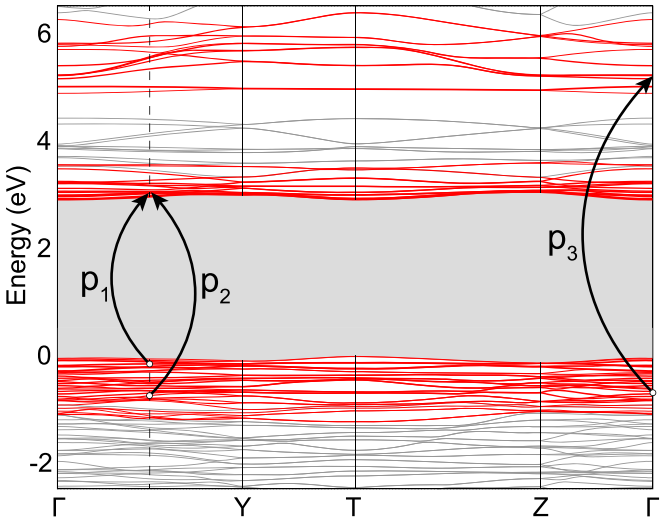

Figure 6. Calculated KTP band structure (DFT-PBEsol). Electronic transitions and states that dominate the dielectric function are highlighted.

transitions between O 2*p* and Ti 3*d* states. This suggests that the strong optical anisotropy of KTP is related to the orientation and placement of the TiO_6 octahedra, which lifts the energy degeneracy of the O 2*p* states. In order to verify this assumption, we partially symmetrize these octahedra by enforcing an additional translational symmetry along [100], allowing to bisect the KTP lattice constant *a*. The resulting artificial KTP cell is tetragonal, with equal lattice constants *a* and *b*, see figure 7. Indeed, for this more symmetric configuration, the splitting between peaks p_1 and p_2 vanishes for all three diagonal components of $\varepsilon(\omega)$. Moreover, the *xx* and *yy* components are now equal, as shown by the dashed lines in figure 5. However, the anisotropy between *xx*/*yy* and *zz* remains, since the density of TiO_6 octahedra along the respective directions differs. Similar observations were made earlier for bismuth titanate ($Bi_4Ti_3O_{12}$)[44].

The IPA spectra calculated here can be compared with previous calculations on the same level of theory [13, 20]. Both studies report DFT calculations within the GGA using the relativistic full-potential linearized augmented-plane-wave method, but arrive at somewhat different results: Reshak *et al* [13], utilizing the Engel–

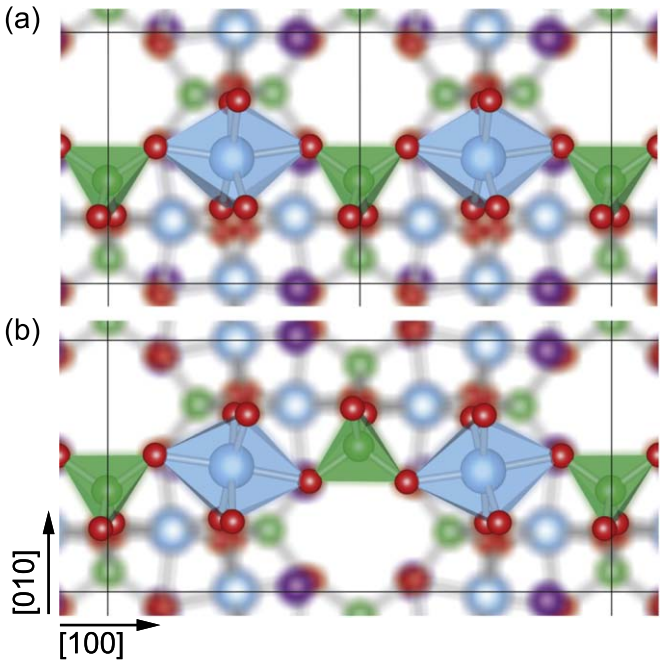

Figure 7. Geometry of TiO_6–PO_4 polyhedra strands (a) within an artificial, partially symmetrized structure of KTP with smaller, tetragonal unit cell (see text) and (b) within orthorhombic bulk KTP. Color coding as in figure 1. Unit-cell boundaries are indicated in black.

Vosko GGA functional [45], find a sharply peaked absorption onset, which is followed by a weak shoulder and a minor peak for $\varepsilon_{xx}/\varepsilon_{yy}$ and ε_{zz}, respectively. In contrast, the more recent calculations by Ghoohestani *et al* [20], utilizing PBEsol and a modified Becke-Johnson functional [46], predict an absorption onset characterized by a minor feature followed by a major peak for ε_{xx} and ε_{zz}. In the case of ε_{yy} a single peak is predicted. The findings of Ghoohestani *et al* [20] are essentially reproduced by the present IPA calculations regarding the line shapes and peak positions as well as the relative peak heights.

A spectral blueshift by more than 2 eV results from the inclusion of quasiparticle effects within the IQA, as shown by the blue lines in figure 5. It positions the first absorption peak at about 6 eV. A redshift by about 1.5 eV results from the inclusion of excitonic and local-field effects in the optical response upon solving the BSE, see the red lines in figure 5. Additionally, the p_2 peak in $\varepsilon_{zz}(\omega)$—which was transformed into a weak shoulder upon applying self-energy corrections—sharpens again if excitonic effects are included. Obviously, the electron-hole interaction partially compensates the quasiparticle effects in the KTP optical response.

The measured average reflectivity reported by Reshak *et al* [13] is compared with the average reflectivity obtained from the dielectric function calculated on the IPA, IQA, and BSE level of theory in figure 8. Clearly, the reflectivity onset calculated within IPA drastically underestimates the experimental findings. This is evidence for the occurrence of large self-energy effects neglected in previous electronic-structure calculations for KTP. On the other hand, the reflectivity obtained from the quasiparticle band structure in the *GW* approximation overestimates the optical transition energies by more than 1 eV. Only the inclusion of electron-hole attraction effects within the BSE leads to a roughly correct alignment with the measured data on the energy axis. The comparison between experiment and theory in figure 8 thus clearly demonstrates the importance of many-body effects for the KTP excited-state properties.

On the other hand, it has to be said that the quantitative agreement between the measured reflectivity and the BSE calculations is clearly not perfect. The onset of the measured reflectivity is underestimated in magnitude and overestimated in energy. The second pronounced reflectivity peak measured at about 5.3 eV is visible only as a weak shoulder in the BSE spectrum. At this point we can only speculate about the reasons. The present calculations neglect zero-point motion and thermal lattice vibrations that are known to lower optical transition energies. This may partially explain the blueshift of the BSE spectrum in comparison to the measured data [41]. Moreover, KTP crystals grown by the traditional flux method, such as used in [13], solidify in a broad homogeneity range, which may not reflect the stoichiometric composition. In fact, the potassium and titanium deviation from stoichiometry may vary within a few atomic percent [7, 47]. Therefore, it cannot be excluded that the remaining discrepancy between experiment and theory is at least partially related to point defects and stoichiometry deviations not included in the present calculations. In fact, defect states are expected to

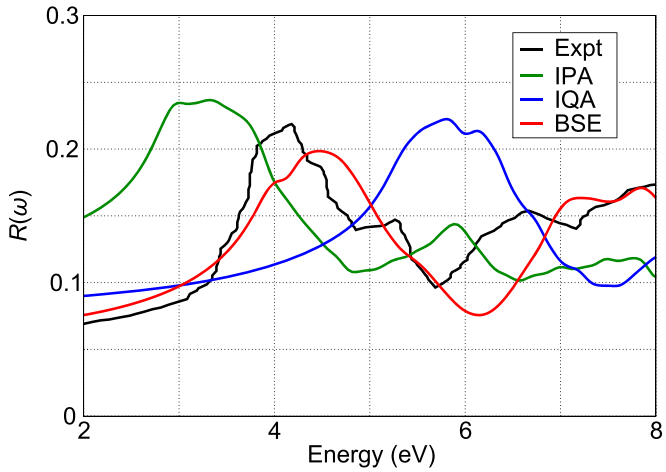

Figure 8. Average reflectivity of KTP calculated on the IPA, IQA and BSE level of theory in comparison to experiment (black line) [13].

redistribute oscillator strengths and are hence a plausible explanation for some deviations between the BSE results and experiments.

Conclusions

Band-structure and optical-response calculations were performed for potassium titanyl phosphate. The calculations show that the electronic transport band gap is much larger than concluded from previous studies. Its lower bound can be expected to be about 5.23 eV. At the same time, the optical band gap is affected by a large exciton binding energy of about 1.5 eV. This demonstrates, that many-body effects are of crucial importance for the KTP excited-state properties. Furthermore, the present calculations show the sensitivity of the KTP optical response with respect to its structural details: the optical anisotropy and peak splitting of the absorption onset is demonstrated to be caused by the orientation and arrangement of the TiO_6 octahedra within the unit cell.

Acknowledgments

Numerical calculations were performed using grants of computer time from the Paderborn Center for Parallel Computing (PC^2) and the HLRS Stuttgart. The Deutsche Forschungsgemeinschaft (DFG) is acknowledged for financial support—project number 231447078—TRR 142.

ORCID iDs

S Neufeld https://orcid.org/0000-0002-7693-098X
A Bocchini https://orcid.org/0000-0002-2134-3075
Arno Schindlmayr https://orcid.org/0000-0002-4855-071X
W G Schmidt https://orcid.org/0000-0002-2717-5076

References

[1] Veithen M, Gonze X and Ghosez P 2005 *Phys. Rev.* B **71** 125107
[2] Bierlein J D and Arweiler C B 1986 *Appl. Phys. Lett.* **49** 917
[3] Shur V Y, Pelegova E V, Akhmatkhanov A R and Baturin I S 2016 *Ferroelectrics* **496** 49
[4] Sorokina N I and Voronkova V I 2007 *Crystallogr. Rep.* **52** 80
[5] Bierlein J D and Vanherzeele H 1989 *J. Opt. Soc. Am.* B **6** 622
[6] Zumsteg F C, Bierlein J D and Gier T E 1976 *J. Appl. Phys.* **47** 4980
[7] Roth M 2010 *Springer Handbook of Crystal Growth* (Berlin: Springer) pp 691–723
[8] Roelofs M G, Suna A, Bindloss W and Bierlein J D 1994 *J. Appl. Phys.* **76** 4999
[9] Zukauskas A, Pasiskevicius V and Canalias C 2013 *Opt. Express* **21** 1395
[10] Thomas P A, Baldwin A, Dupree R, Blaha P, Schwarz K, Samoson A and Gan Z H 2004 *J. Phys. Chem.* B **108** 4324
[11] Munowitz M, Jarman R H and Harrison J F 1993 *Chem. Mater.* **5** 1257
[12] Munowitz M, Jarman R H and Harrison J F 1993 *Chem. Mater.* **5** 661
[13] Reshak A H, Kityk I V and Auluck S 2010 *J. Phys. Chem.* B **114** 16705
[14] Dudelzak A, Proulx P-P, Denks V, Mürk V and Nagirnyi V 2000 *J. Appl. Phys.* **87** 2110

[15] Sheik-Bahae M, Hutchings D C, Hagan D J and Stryland E W Van 1991 *IEEE J. Quantum Electron.* **27** 1296
[16] Li H P, Kam C H, Lam Y L and Ji W 2001 *Opt. Mater.* **15** 237
[17] Desalvo R, Said A A, Hagan D J, Van Stryland E W and Sheik-Bahae M 1996 *IEEE J. Quantum Electron.* **32** 1324
[18] Lowther J E, Manyum P and Suebka P 2005 *Phys. Status Solidi* b **242** 1392
[19] Zhang Y, Leng Y, Liu J, Ji N, Duan X, Li J, Zhao X, Wang J and Jiang H 2015 *CrystEngComm* **17** 3793
[20] Ghoohestani M, Arab A, Hashemifar S J and Sadeghi H 2018 *J. Appl. Phys.* **123** 015702
[21] Ching W Y and Xu Y N 1991 *Phys. Rev.* B **44** 5332
[22] Albrecht S, Reining L, Del Sole R and Onida G 1998 *Phys. Rev. Lett.* **80** 4510
[23] Rohlfing M and Louie S G 1998 *Phys. Rev. Lett.* **81** 2312
[24] Rohlfing M and Louie S G 1998 *Phys. Rev. Lett.* **80** 3320
[25] Hahn P H, Schmidt W G and Bechstedt F 2001 *Phys. Rev. Lett.* **88** 016402
[26] Schmidt W G, Albrecht M, Wippermann S, Blankenburg S, Rauls E, Fuchs F, Rödl C, Furthmüller J and Hermann A 2008 *Phys. Rev.* B **77** 035106
[27] Riefer A, Sanna S, Schindlmayr A and Schmidt W G 2013 *Phys. Rev.* B **87** 195208
[28] Hybertsen M S and Louie S G 1986 *Phys. Rev.* B **34** 5390
[29] Bechstedt F 2015 *Many-Body Approach to Electronic Excitations: Concepts and Applications* (Berlin: Springer)
[30] Hedin L 1965 *Phys. Rev.* **139** A796
[31] Onida G, Reining L and Rubio A 2002 *Rev. Mod. Phys.* **74** 601
[32] Kresse G and Furthmüller J 1996 *Phys. Rev.* B **54** 11169
[33] Perdew J P, Ruzsinszky A, Csonka G I, Vydrov O A, Scuseria G E, Constantin L A, Zhou X and Burke K 2008 *Phys. Rev. Lett.* **100** 136406
[34] Kresse G and Joubert D 1999 *Phys. Rev.* B **59** 1758
[35] Shishkin M and Kresse G 2006 *Phys. Rev.* B **74** 035101
[36] Schmidt W G, Glutsch S, Hahn P H and Bechstedt F 2003 *Phys. Rev.* B **67** 085307
[37] Allan D R, Loveday J S, Nelmes R J and Thomas P A 1992 *J. Phys.: Condens. Matter* **4** 2747
[38] Hagerman M E and Poeppelmeier K R 1995 *Chem. Mater.* **7** 602
[39] Norberg S T, Thomas P A and Tucker M G 2011 *J. Phys.: Condens. Matter* **23** 175401
[40] Thomas P A, Glazer A M and Watts B E 1990 *Acta Crystallogr.* B **46** 333
[41] Riefer A, Friedrich M, Sanna S, Gerstmann U, Schindlmayr A and Schmidt W G 2016 *Phys. Rev.* B **93** 075205
[42] Steiner S, Khmelevskyi S, Marsmann M and Kresse G 2016 *Phys. Rev.* B **93** 224425
[43] Riefer A, Weber N, Mund J, Yakovlev D R, Bayer M, Schindlmayr A, Meier C and Schmidt W G 2017 *J. Phys.: Condens. Matter* **29** 215702
[44] Roy A, Prasad R, Auluck S and Garg A 2014 *J. Appl. Phys.* **115** 133509
[45] Engel E and Vosko S H 1993 *Phys. Rev.* B **47** 13164
[46] Becke A D and Johnson E R 2006 *J. Chem. Phys.* **124** 221101
[47] Roth M, Angert N, Tseitlin M and Alexaandrovski A 2001 *Opt. Mater.* **16** 131